# Spin-Dependent Molecule Symmetry at a Pentacene–Co Spinterface

**Yu-Hsun Chu,[†] Chuang-Han Hsu,[†] Chun-I Lu,[†] Hung-Hsiang Yang,[†] Tsung-Han Yang,[†] Chi-Hung Luo,[†] Kai-Jheng Yang,[†] Shih-Hao Hsu,[†] Germar Hoffmann,[†,‡] Chao-Cheng Kaun,[§,‡] and Minn-Tsong Lin*[,†,⊥]**

[†]Department of Physics, National Taiwan University, Taipei 10617, Taiwan, [‡]Department of Physics, National Tsing Hua University, Hsinchu 30013, Taiwan, [§]Research Center for Applied Sciences, Academia Sinica, Taipei 11529, Taiwan, and [⊥]Institute of Atomic and Molecular Sciences, Academia Sinica, Taipei 10617, Taiwan

**ABSTRACT** Incorporating spin-polarized scanning tunneling microscopy (SP-STM) measurements and first-principles calculations, we resolve spin-polarized states and consequent features in a pentacene(PEN)–Co hybrid system. Symmetry reduction of PEN clarifies the PEN adsorption site and the Co stacking methods. Near the Fermi energy, the molecular symmetry is spin-dependently recovered and an inversion of spin-polarization in PEN with respect to Co is observed. The experimental findings and calculation results are interpreted by a $p_z$–d hybridization model, in which spin-dependent bonding–antibonding splitting of molecular orbitals happens at metal–organic spinterfaces.

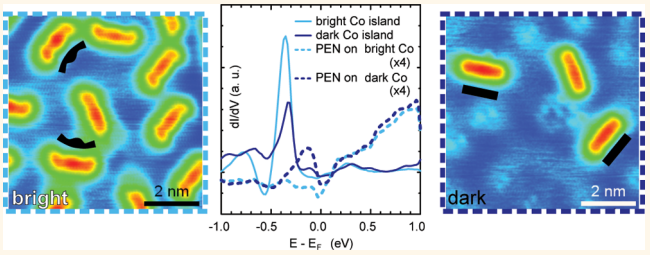


**KEYWORDS:** spin-polarized scanning tunneling spectroscopy · molecular symmetry · pentacene · cobalt island · spinterface · organic-metal hybridization · first-principles calculation

Organic spintronics has drawn much attention since the past decade, because of not only advantages like flexibility and bottom-up fabrications in organic materials for electronics,[1] but also weak spin–orbit coupling, which leads to longer spin coherence distance and time.[2,3] While spin conservation during electron transport is improved in organic materials, organic–ferromagnetic (FM) heterostructures raise additional issues of spinterfaces.[4,5] Molecules become spin-polarized after attaching to magnetic surfaces, which depends on interfacial interactions. The spin-polarized states can influence spin injection efficiency and result in phenomena such as sign reversal of magnetoresistance in spin valves.[6] In organic electronics, $\pi$-conjugations allow electrons to transport through stacked molecular layers.[7] One famous $\pi$-conjugated molecule is PEN ($C_{22}H_{14}$), which is composed of five linear-fused benzene rings (top inset in Figure 1a). Used as a p-type organic semiconductor in thin film transistors,[8,9] PEN also plays a successful role in spin valves,[10,11] in which interfacial interactions with PEN influence magnetic properties in FM Co layers[12] and magnetoresistance performance.[11] Surprisingly, detailed investigations into PEN–FM spinterfaces are essential but still lacking.

In this article, to resolve the PEN–FM spinterface at the nanoscale, we visualize spin-distribution within single PEN molecules *via* spin-polarized scanning tunneling microscopy (SP-STM) and spin-polarized scanning tunneling spectroscopy (SP-STS),[13,14] which have been used to resolved intramolecular spin-distribution.[15,16] Deposited on FM Co nanoislands on Cu(111),[17–21] the PEN symmetry not only clarifies stacking methods of Co islands, but also appears spin-dependent near the Fermi level, which emphasizes the necessity of introducing spin-dependent measurements in studies in molecular structures. Coexisting PEN spin-polarization opposite to Co agrees with the $p_z$–d Zener exchange mechanism recently introduced for hybridizations between molecule $\pi(p_z)$ orbitals and surface d states.[22,23] Our *ab initio* density functional theory (DFT) calculations shows spin-dependent splitting of a PEN molecular orbital (MO). Comparing calculations and experimental results, we conclude that the spin-selected PEN symmetries result from the spin-dependent antibonding state in $p_z$–d

* Address correspondence to mtlin@phys.ntu.edu.tw.

Received for review March 4, 2015 and accepted June 17, 2015.

**Published online June 17, 2015**
**10.1021/acsnano.5b03117**

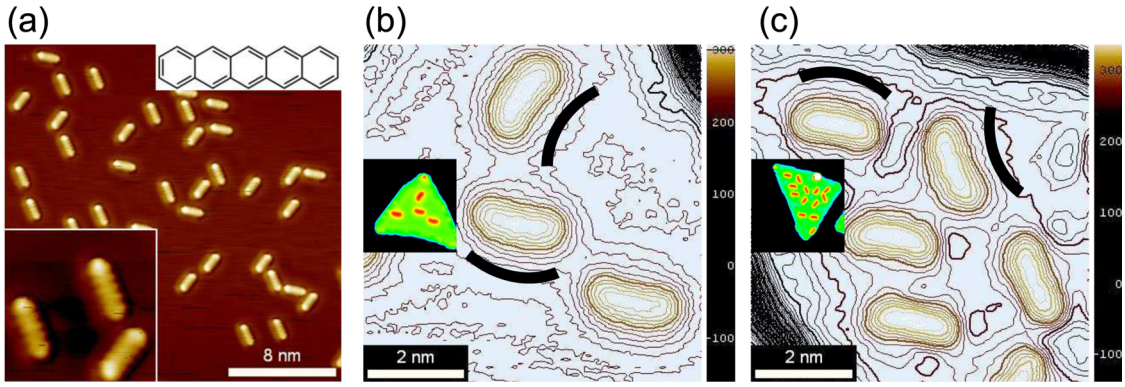


**Figure 1. (a) STM image of PEN molecules adsorbed on the Cu(111) surface. Protrusions inside the molecules resemble the LUMO of PEN (in the zoom-in inset, 4 nm × 4 nm, $V_{bias}$: 0.5 V). PEN chemical structure is shown in the top-right inset. (b and c) Contour maps of PEN molecules on a faulted Co island and on an unfaulted Co island on Cu(111), respectively (height interval: 8 pm), in which the bending of molecules is revealed as marked. Zoom-out images containing the whole islands are in the insets. (Inset in (b), 16 × 16 nm$^2$, $V_{bias}$ = 0.5 V; inset in (c), 20 × 20 nm$^2$, $V_{bias}$ = 0.5 V).**

hybridizations, which also contributes to the measured PEN spin-polarization.

## RESULTS AND DISCUSSION

For comparison, we first deposit PEN on pristine Cu(111) at submonolayer coverage. Isolated PEN molecules exhibit three adsorption orientations as shown in Figure 1a with visible intramolecular protrusions. The protrusion pattern is in consistence with a previous study of Lagoute *et al.* and corresponds to the lowest unoccupied molecular orbital (LUMO) of PEN.[24] Lagoute *et al.* have also revealed that PEN aligns its long axis along ⟨110⟩ on Cu(111) and adsorbs at the hcp hollow site, at which the central benzene ring is located. Although Cu atoms under PEN are asymmetric along the long axis, the $C_{2v}$ symmetry of PEN remains apparent due to mild hybridizations with Cu.

Depositing PEN on Co nanoislands on Cu(111), we observe a depopulation of the bare Cu surface, and a gathering of PEN molecules on the islands. This indicates stronger hybridizations of PEN on Co than on Cu. PEN molecules stay isolated from each other and follow the same adsorption orientations as on Cu(111), but the free molecule $C_{2v}$ symmetry is reduced to $C_v$. Figure 1b,c shows PEN on a Co island with faulted and unfaulted stacking on Cu(111), respectively. (Stacking fault is determined in STS by the energy positions of the characteristic peak of the $d_{z^2}$ state at about −0.3 V and by the ratio of island numbers pointing up *vs* islands pointing down. The ratio is around 1:2 and agrees with the ratio of the faulted to the unfaulted islands in literatures. The statistical result is from 322 islands.) On both islands, PEN molecules are bent, possessing only a mirror symmetry with respect to the PEN short axis. Top and bridge sites are excluded from possible adsorption sites because of the lack of rotational symmetries and the existence of the mirror symmetry (see Supporting Information). As a result, the most possible adsorption site with a high symmetry is the hollow site. Compared to the PEN−Cu adsorption, stronger hybridizations with Co reflect asymmetric arrangements of Co atoms underneath and distort the PEN geometry.

It is worth noting that two kinds of hollow sites exist: hcp and fcc hollow sites, which are categorized by whether or not there is an atom in the bottom Co layer. If both hollow sites were PEN adsorption sites, there would be six PEN geometries separated by a 60 degree rotation on all islands. However, without perturbations such as adsorbate attachment or island boundaries, the convex side of PEN molecules always aims at the island edges instead of the corners (Figure 1b,c). That is, on the faulted islands, only three PEN geometries separated by 120° can be found, whereas the other three exist on the unfaulted islands. The results suggest that, influenced by the bottom-layer Co, PEN is adsorbed at only one kind of hollow sites for each stacking method. In DFT calculations, we build four possible stacking methods of Co and the fcc hollow site always results in lower PEN adsorption energy, which supports the aforementioned speculation that only one kind of hollow site works as the PEN adsorption site on Co. Figure 2a is one optimized structure of the four calculated systems, in which the Co layers follow the unfaulted stacking and PEN locates at the fcc hollow site. (Although the metallic system is in a thin film structure in calculations, the characteristic surface states of Co are successfully reproduced. The same method has been used in literatures as ref 19.) The optimized PEN in Figure 2a is found asymmetrically distorted from the side view. Combining Tersoff−Hamann theory[25] and DFT calculations, we simulate STM images (Figure 2b), in which the bending of the molecule is reproduced.

However, drawing four PEN adsorption situations in Figure 2c−f, we find that it is impossible for all of them to be valid. While PEN convex sides point to the island edges in STM images, Figure 2e,f gives contrary results.

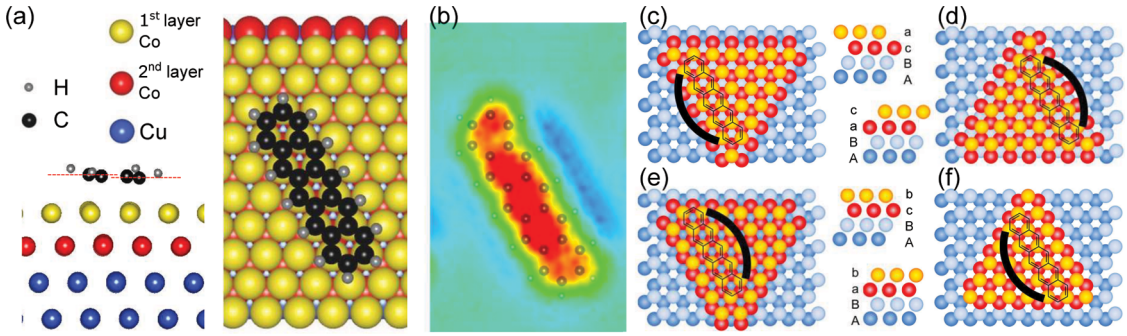


**Figure 2. (a) Optimized structure of a PEN molecule adsorbed on bilayer Co on bilayer Cu obtained from DFT calculations. The stacking order is acBA, starting from the top Co to the bottom Cu layer, which are represented by lower-case and capital letters, respectively. PEN is asymmetric along the long axis in the side view. (b) Simulated STM image of the system in (a) at −0.1 eV with the PEN atomic structure. (Height for simulation: 4 Å.) (c−f) Schematics of PEN adsorption on Co islands of 4 stacking models. Thick black lines indicate the bending directions of PEN molecules. It can be seen that only in (c) and (d) the PEN convex direction matches experimental results in Figure 1.**

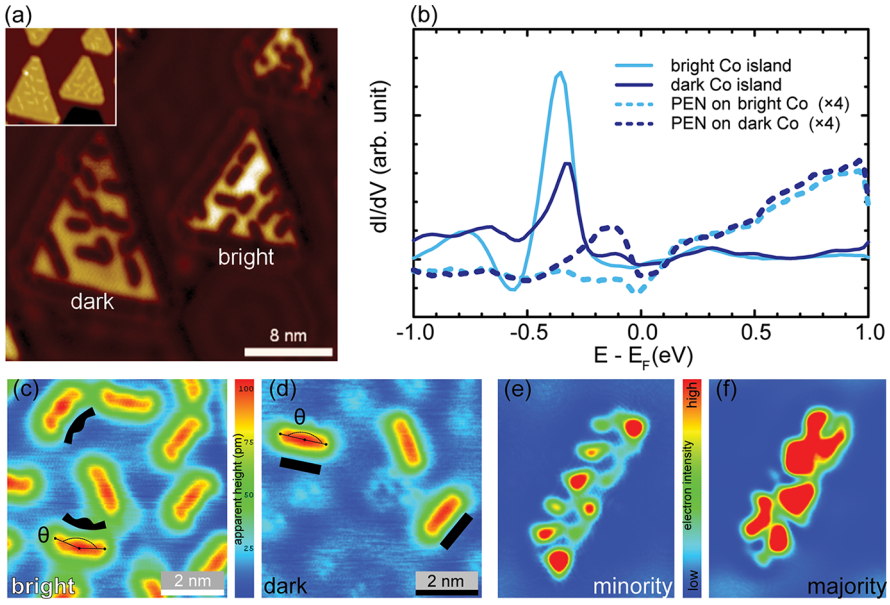


**Figure 3. An SP-STS (a) map ($V_{bias}$: −0.3 V) and (b) curves measured on the marked islands. Co islands exhibit strong contrast due to the minority $d_{z^2}$ state at −0.3 eV as in ref 31. Inset in (a): topography of the area in (a) taken at the same energy. (c and d) SP-STM images taken at −0.1 V, at which a new spin-polarized state occurs. On islands with opposite magnetization orientations, PEN exhibits different geometries. Black marks emphasize features in shape of the PEN molecules and the angle $\theta$ between line segments is measured for approach to symmetry determinations. (e) Minority and (f) majority integrated PDOS of PEN on Co from 0 to −0.1 eV, in which molecule shapes are consistent with (c) and (d), respectively.**

Therefore, the correct stacking methods for the Co islands are acBA and caBA instead of the other two (lower-case and capital letters represent Co and Cu, respectively, in the order from top to bottom). In fact, despite of intense studies on the Co/Cu(111) system, concrete determination of the top-layer Co stacking is rare.[26] Molecular symmetry reduction leads to a new way to solve stacking ambiguity in systems like Co nanoislands.

To study magnetic properties of PEN adsorbed on Co, we utilize SP-STM to achieve direct spin-resolved measurements. Co nanoislands are FM nanostructures with out-of-plane magnetic anisotropy, and output different d*I*/d*V* signals with different magnetization orientations in SP-STS maps. In Figure 3a, contrast of the Co islands appears at −0.3 eV due to opposite $d_{z^2}$ minority states, which also contributes to the characteristic peak at −0.3 eV in SP-STS curves (Figure 3b). On PEN molecules, we find a new spin-polarized state at around −0.1 eV. Contrary to the Co $d_{z^2}$ minority state, the new state has higher intensity on the dark island than on the bright island in Figure 3a, which indicates that it is a majority state. Therefore, spin polarization right below the Fermi level is locally reversed *via* PEN adsorption on Co.

PEN molecules also exhibit spin-dependent symmetries at −0.1 eV in SP-STM images. On the bright island in Figure 3a, PEN molecules are bent and divided into three sections (Figure 3c), while they are more oval on the dark island (Figure 3d). We defined a bending

angle $\theta$, which is marked on Figure 3c,d, to represent the extent of PEN symmetry deviation from the original $C_{2v}$ one. The averaged angle $\theta$ between segments from the molecule center to both ends is 157.3° and 173.5° for PEN on the bright and the dark islands, respectively, while for a perfect $C_{2v}$ symmetry, $\theta$ should be 180°. (Statistical distributions of $\theta$ of PEN on islands with opposite magnetization orientations are shown in Supporting Information.) The results indicate that near the Fermi level, the symmetry of PEN is spin-dependent, which almost recovers $C_{2v}$ symmetry on the dark island.

On the dark island at −0.1 eV, the PEN majority states contribute more to SP-STM measurements than on the bright island; thus, the symmetry recovery of PEN should result from the majority states. We resolve the electron distribution in PEN spin-dependently by calculating integrated partial density of states (PDOS) of the new spin-polarized state in adsorbed PEN. In the [−0.1, 0] eV energy interval, minority electrons have a curved distribution with high intensity at both ends and the center (Figure 3e), whereas majority electrons present a more oval shape (Figure 3f). In spite of the existence of geometric symmetry-reduction, molecules can stay symmetric in STM images because of a symmetric electron distribution.[27,28] The DFT calculations suggest that our SP-STM findings in Figure 3c,d originate from electron distributions with different spin orientations.

Figure 4a shows the calculated Co $d_{z^2}$ PDOS without and with PEN adsorption. While most of the d states vary slightly (see Supporting Information), the $d_{z^2}$ states are broadened and shifted by PEN adsorption. Solving the PDOS of PEN, we find that $p_z$ MOs are dominant in the energy range in Figure 4, whereas the in-plane p orbitals ($p_x$, $p_y$) contribute very little (see Supporting Information). Due to proximity in space, the out-of-plane orbitals are easy to overlap with each other; thus, hybridizatinos between C $p_z$ and Co $d_{z^2}$ states are as expected. Acting as an electron donor, Co transfers 2.16 $e^-$ to PEN, which largely reduce amplitude of the Co $d_{z^2}$ states near the Fermi level. In Figure 4b, perceptible hybridizations are found in the [−0.8, 0.4] eV energy interval, in which C $p_z$ and Co $d_{z^2}$ majority states share similar PDOS distributions. In this energy range, the PEN molecule is majority-dominant and opposite to the pristine Co. This inversion of spin-polarization is exactly what we have experimentally confirmed in Figure 3b using SP-STM.

Examining the composition of PEN $p_z$ states by projecting the $p_z$ electron distribution to different PEN MOs, we find that the highest occupied MO (HOMO) contributes the most in the [−0.1, 0] eV energy interval. The HOMO is broadened due to hybridization with Co; furthermore, the majority HOMO is divided into two energy regime, whereas minority HOMO remains as one (marked in Figure 4b). The spin-dependent

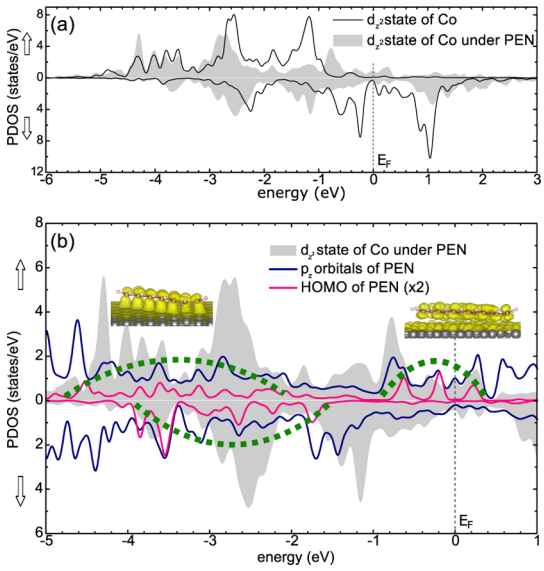


**Figure 4. (a) Calculated PDOS of surface Co with and without PEN above. The Co $d_{z^2}$ states change the distribution after PEN adsorption. (b) PDOS of Co $d_{z^2}$ states after PEN adsorption and PEN $p_z$ orbitals. Correspondence in majority PEN $p_z$ and Co $d_{z^2}$ states exists near the Fermi level. The PEN HOMO projection is put on the plot as well. Green dashed lines indicate the distribution of the PEN HOMO. Insets: integrated PDOS in the [−3, −2.6] and [−0.4, 0] eV energy intervals, in which bonding and antibonding features are shown, respectively.**

MO splitting agrees with the $p_z$−d Zener exchange mechanism recently introduced to organic-FM hybridizations.[22,29,30] The model predicts that the $p_z$ majority MO splits into bonding and antibonding states hybridizing with the substrate d states, while the minority MO has weaker hybridization. To clarify the PEN HOMO bonding methods, we illustrate majority integrated PDOS in the [−3, −2.6] and [−0.4, 0] eV energy intervals. Shown in the insets of Figure 4b, the calculated integrated PDOS in the [−0.4, 0] energy range has repulsion of electrons between Co and the PEN molecules, which indicates that the HOMO forms an antibonding state with the Co support. On the contrary, the PEN molecule and Co share the electrons in between and form a bonding state in the [−3, −2.6] eV energy range. Therefore, we conclude that the PEN HOMO hybridizes with the Co substrate based on the $p_z$−d Zener exchange mechanism. In addition, the more symmetric integrated PDOS in Figure 3f agrees with the antibonding feature since the electron distribution in space is less perturbed by Co arrangement underneath. The result supports the experimentally observed spin-dependent molecule symmetry, which can only be observed *via* SP-STM capable of making spin-selective maps.

## CONCLUSION

The symmetry reduction of PEN on Co nanoislands has been investigated from the origin to the deductions based on it. On the basis of the bending of the

PEN geometry, we determine the PEN adsorption site (the fcc hollow site) and the stacking methods of the Co islands *via* combined experimental and theoretical works. Using SP-STM, we find not only spin-polarization locally reversed by PEN, but also spin-dependent molecule symmetries. From DFT calculations, we interpret the experimental results as a consequence of the $p_z$−d hybridization between PEN and Co. While the minority HOMO is only broadened, the majority HOMO is split into the bonding and the antibonding states. The antibonding majority HOMO contributes to the reversed spin-polarization at around −0.1 eV, and agrees with the spin-dependent PEN symmetries observed in the same energy range. Our observations of spin-dependent molecular symmetries introduce an important and intrinsic factor in determining molecular symmetries, namely, spin, which should be considered as well as geometric and electronic status. Antibonding states from $p_z$−d Zener exchange mechanism help molecules to recover symmetry spin-dependently regardless of structure distortion, and show a concise way to predict and manipulate molecular spin-distribution near the Fermi level through deposition of $\pi$-conjugated molecule on magnetic substrates.

## METHOD

All experiments are performed in an Omicron multifunction chamber in ultrahigh vacuum with low-temperature STM. Experiments start from cleaning the Cu(111) substrate by 1 keV $Ar^+$ sputtering and subsequent annealing at around 700 K. Removal of impurities is confirmed by Auger electron spectroscopy, and a flat Cu(111) surface with monolayer-high terraces is observed in STM images. Triangular Co islands form on Cu(111) at room temperature after deposition of Co with the molecular beam epitaxy technique. PEN molecules are deposited using a homemade thermal evaporation gun at deposition temperature around 420 K. The samples are transferred into the low-temperature STM at 4.5 K immediately after above *in situ* preparations to suppress Cu intermixing. We use W tips and Co-coated Fe−Mn−C-alloy tips[31] for STM and SP-STM, respectively.

For DFT calculations, the Quantum ESPRESSO package is used,[32] with a plane-wave basis set, within generalized gradient approximation[33] for exchange-correlation interactions. The van der Waals interaction is also employed.[34−36] Two layers of Co are designed to sit on two layers of Cu following the fcc (111) direction, and PEN is put on the Co layers with adsorption sites described in the Results and Discussion section. Convergence with respect to the number of Cu layers has been confirmed in a previous work of Mn-phthalocyanine on the Co islands,[37] in which three and two layers of Cu provide almost the same results in calculations. The spacing between two slabs is larger than 20.0 Å. The cut off kinetic energy and charge density are 25 and 250 Ry, respectively. The convergence conditions are that the force acting on each atom is smaller than $10^{-3}$ Ry/Å and the self-consistent converged criterion is $10^{-5}$ eV. Combining Tersoff−Hamann theory,[25] simulated STM is performed at reasonable height of 4 Å, which, according to calculations, is enough to ignore tip−sample hybridizations for W and C in experiments.[38,39] We use the Γ reciprocal point to sample the Brillouin zone. Charge transfer is calculated with Bader charge analysis.[40−42]

*Conflict of Interest:* The authors declare no competing financial interest.

*Acknowledgment.* This work was supported by the National Science Council of Taiwan through Grant No. NSC 101-2112-M-002-024-MY3 and the Ministry of Science and Technology of Taiwan through Grant No. MOST 103-2120-M-002-001.

*Supporting Information Available:* Schematics of PEN at different adsorption sites, statistical distributions of the bending angle $\theta$, and *ab initio* calculation results of all d states of Co and p orbitals of pentacene. The Supporting Information is available free of charge on the ACS Publications website at DOI: 10.1021/acsnano.5b03117.

## REFERENCES AND NOTES

1. Kelley, T. W.; Baude, P. F.; Gerlach, C.; Ender, D. E.; Muyres, D.; Haase, M. A.; Vogel, D. E.; Theiss, S. D. Recent Progress in Organic Electronics: Materials, Devices, and Processes. *Chem. Mater.* **2004**, *16*, 4413–4422.
2. Dediu, V.; Murgia, M.; Matacotta, F.; Taliani, C.; Barbanera, S. Room Temperature Spin Polarized Injection in Organic Semiconductor. *Solid State Commun.* **2002**, *122*, 181–184.
3. Xiong, Z. H.; Wu, D.; Shi, J. Giant Magnetoresistance in Organic Spin-Valves. *Nature* **2004**, *427*, 821–824.
4. Sanvito, S. Molecular Spintronics: The Rise of Spinterface Science. *Nat. Phys.* **2010**, *6*, 562–564.
5. Raman, K. V.; Kamerbeek, A. M.; Mukherjee, A.; Atodiresei, N.; Sen, T. K.; Lazić, P.; Caciuc, V.; Michel, R.; Stalke, D.; Mandal, S. K.; et al. Interface-Engineered Templates for Molecular Spin Memory Devices. *Nature* **2013**, *493*, 509–513.
6. Barraud, C.; Seneor, P.; Mattana, R.; Fusil, S.; Bouzehouane, K.; Deranlot, C.; Graziosi, P.; Hueso, L.; Bergenti, I.; Dediu, V.; et al. Unravelling the Role of the Interface for Spin Injection into Organic Semiconductors. *Nat. Phys.* **2010**, *6*, 615–620.
7. Coropceanu, V.; Cornil, J.; da Silva Filho, D. A.; Olivier, Y.; Silbey, R.; Brédas, J.-L. Charge Transport in Organic Semiconductors. *Chem. Rev.* **2007**, *107*, 926–952.
8. Lin, Y.-Y.; Gundlach, D. J.; Nelson, S.; Jackson, T. Stacked Pentacene Layer Organic Thin-Film Transistors with Improved Characteristics. *IEEE Electron Device Lett.* **1997**, *18*, 606–608.
9. Puigdollers, J.; Voz, C.; Orpella, A.; Quidant, R.; Martín, I.; Vetter, M.; Alcubilla, R. Pentacene Thin-Film Transistors with Polymeric Gate Dielectric. *Org. Electron.* **2004**, *5*, 67–71.
10. Ikegami, T.; Kawayama, I.; Tonouchi, M.; Nakao, S.; Yamashita, Y.; Tada, H. Planar-Type Spin Valves based on Low-Molecular-Weight Organic Materials with $La_{0.67}Sr_{0.33}MnO_3$ Electrodes. *Appl. Phys. Lett.* **2008**, *92*, 153304.
11. Hong, J.-Y.; Chang, Y.-M.; Chuang, C.-H.; Li, K.-S.; Jhang, Y.-C.; Shiu, H.-W.; Chen, C.-H.; Chiang, W.-C.; Lin, M.-T. Depth Profiling Photoelectron-Spectroscopic Study of an Organic Spin Valve with a Plasma-Modified Pentacene Spacer. *J. Phys. Chem. C* **2012**, *116*, 21157–21161.
12. Chan, Y.-L.; Hung, Y.-J.; Wang, C.-H.; Lin, Y.-C.; Chiu, C.-Y.; Lai, Y.-L.; Chang, H.-T.; Lee, C.-H.; Hsu, Y. J.; Wei, D. H. Magnetic Response of an Ultrathin Cobalt Film in Contact with an Organic Pentacene Layer. *Phys. Rev. Lett.* **2010**, *104*, 177204.
13. Bode, M. Spin-Polarized Scanning Tunnelling Microscopy. *Rep. Prog. Phys.* **2003**, *66*, 523–582.
14. Wiesendanger, R. Spin Mapping at the Nanoscale and Atomic Scale. *Rev. Mod. Phys.* **2009**, *81*, 1495–1550.
15. Brede, J.; Atodiresei, N.; Kuck, S.; Lazić, P.; Caciuc, V.; Morikawa, Y.; Hoffmann, G.; Blügel, S.; Wiesendanger, R. Spin- and Energy-Dependent Tunneling through a Single Molecule with Intramolecular Spatial Resolution. *Phys. Rev. Lett.* **2010**, *105*, 047204.
16. Schwöbel, J.; Fu, Y.; Brede, J.; Dilullo, A.; Hoffmann, G.; Klyatskaya, S.; Ruben, M.; Wiesendanger, R. Real-Space

Observation of Spin-Split Molecular Orbitals of Adsorbed Single-Molecule Magnets. *Nat. Commun.* **2012**, *3*, 953.
17. de la Figuera, J.; Prieto, J. E.; Ocal, C.; Miranda, R. Scanning-Tunneling-Microscopy Study of the Growth of Cobalt on Cu(111). *Phys. Rev. B* **1993**, *47*, 13043–13046.
18. Vázquez de Parga, A. L.; García-Vidal, F. J.; Miranda, R. Detecting Electronic States at Stacking Faults in Magnetic Thin Films by Tunneling Spectroscopy. *Phys. Rev. Lett.* **2000**, *85*, 4365–4368.
19. Diekhöner, L.; Schneider, M. A.; Baranov, A. N.; Stepanyuk, V. S.; Bruno, P.; Kern, K. Surface States of Cobalt Nanoislands on Cu(111). *Phys. Rev. Lett.* **2003**, *90*, 236801.
20. Pietzsch, O.; Kubetzka, A.; Bode, M.; Wiesendanger, R. Spin-Polarized Scanning Tunneling Spectroscopy of Nanoscale Cobalt Islands on Cu(111). *Phys. Rev. Lett.* **2004**, *92*, 057202.
21. Pietzsch, O.; Okatov, S.; Kubetzka, A.; Bode, M.; Heinze, S.; Lichtenstein, A.; Wiesendanger, R. Spin-Resolved Electronic Structure of Nanoscale Cobalt Islands on Cu(111). *Phys. Rev. Lett.* **2006**, *96*, 237203.
22. Atodiresei, N.; Brede, J.; Lazić, P.; Caciuc, V.; Hoffmann, G.; Wiesendanger, R.; Blügel, S. Design of the Local Spin Polarization at the Organic-Ferromagnetic Interface. *Phys. Rev. Lett.* **2010**, *105*, 066601.
23. Callsen, M.; Caciuc, V.; Kiselev, N.; Atodiresei, N.; Blügel, S. Magnetic Hardening Induced by Nonmagnetic Organic Molecules. *Phys. Rev. Lett.* **2013**, *111*, 106805.
24. Lagoute, J.; Kanisawa, K.; Fölsch, S. Manipulation and Adsorption-Site Mapping of Single Pentacene Molecules on Cu(111). *Phys. Rev. B* **2004**, *70*, 245415.
25. Tersoff, J.; Hamann, D. R. Theory of the Scanning Tunneling Microscope. *Phys. Rev. B* **1985**, *31*, 805–813.
26. Ignatiev, P. A.; Stepanyuk, V. S.; Niebergall, L.; Bruno, P.; Berakdar, J. Interplay of Electronic, Magnetic and Structural Properties of Surface-Supported Clusters. *Eur. Phys. J. D* **2007**, *45*, 547–551.
27. Chang, S.-H.; Kuck, S.; Brede, J.; Lichtenstein, L.; Hoffmann, G.; Wiesendanger, R. Symmetry Reduction of Metal Phthalocyanines on Metals. *Phys. Rev. B* **2008**, *78*, 233409.
28. Heinrich, B. W.; Iacovita, C.; Brumme, T.; Choi, D.-J.; Limot, L.; Rastei, M. V.; Hofer, W. A.; Kortus, J.; Bucher, J.-P. Direct Observation of the Tunneling Channels of a Chemisorbed Molecule. *J. Phys. Chem. Lett.* **2010**, *1*, 1517–1523.
29. Kanamori, J.; Terakura, K. A General Mechanism Underlying Ferromagnetism in Transition Metal Compounds. *J. Phys. Soc. Jpn.* **2001**, *70*, 1433–1434.
30. Dietl, T. Ferromagnetic Semiconductors. *Semicond. Sci. Technol.* **2002**, *17*, 377–392.
31. Hsu, P.-J.; Lu, C.-I.; Chen, S.-W.; Hsueh, W.-J.; Chu, Y.-H.; Hsu, C.-H.; Butler, C. J.; Lin, M.-T. In situ Magnetization Switching of Magnetic Probes Applied to SpinPolarized Scanning Tunneling Microscopy. *Appl. Phys. Lett.* **2010**, *96*, 142515.
32. Giannozzi, P.; Baroni, S.; Bonini, N.; Calandra, M.; Car, R.; Cavazzoni, C.; Ceresoli, D.; Chiarotti, G. L.; Cococcioni, M.; Dabo, I.; et al. QUANTUM ESPRESSO: A Modular and Open-Source Software Project for Quantum Simulations of Materials. *J. Phys.: Condens. Matter* **2009**, *21*, 395502.
33. Langreth, D. C.; Perdew, J. P. Theory of Nonuniform Electronic Systems. I. Analysis of the Gradient Approximation and a Generalization that Works. *Phys. Rev. B* **1980**, *21*, 5469–5493.
34. Dion, M.; Rydberg, H.; Schröder, E.; Langreth, D. C.; Lundqvist, B. I. Van der Waals Density Functional for General Geometries. *Phys. Rev. Lett.* **2004**, *92*, 246401.
35. Grimme, S. Accurate Description of van der Waals Complexes by Density Functional Theory Including Empirical Corrections. *J. Comput. Chem.* **2004**, *25*, 1463–1473.
36. Grimme, S. Semiempirical GGA-type Density Functional Constructed with a Long-Range Dispersion Correction. *J. Comput. Chem.* **2006**, *27*, 1787–1799.
37. Hsu, C.-H.; Chu, Y.-H.; Lu, C.-I.; Hsu, P.-J.; Chen, S.-W.; Hsueh, W.-J.; Kaun, C.-C.; Lin, M.-T. Spin-Polarized Transport through Single Manganese Phthalocyanine Molecules on a Co Nanoisland. *J. Phys. Chem. C* **2015**, *119*, 3374–3378.
38. Chaika, A.; Nazin, S.; Bozhko, S. Selective STM Imaging of Oxygen-Induced Cu(115) Surface Reconstructions with Tungsten Probes. *Surf. Sci.* **2008**, *602*, 2078–2088.
39. Chaika, A. N.; Nazin, S. S.; Semenov, V. N.; Bozhko, S. I.; Lübben, O.; Krasnikov, S. A.; Radican, K.; Shvets, I. V. Selecting the Tip Electron Orbital for Scanning Tunneling Microscopy Imaging with Sub-Ångström Lateral Resolution. *Europhys. Lett.* **2010**, *92*, 46003.
40. Henkelman, G.; Arnaldsson, A.; Jónsson, H. A Fast and Robust Algorithm for Bader Decomposition of Charge Density. *Comput. Mater. Sci.* **2006**, *36*, 354–360.
41. Sanville, E.; Kenny, S. D.; Smith, R.; Henkelman, G. Improved rid-Based Algorithm for Bader Charge Allocation. *J. Comput. Chem.* **2007**, *28*, 899–908.
42. Tang, W.; Sanville, E.; Henkelman, G. A Grid-based Bader Analysis Algorithm without Lattice Bias. *J. Phys.: Condens. Matter* **2009**, *21*, 084204.